Hindawi Publishing Corporation
Journal of Nanomaterials
Volume 2013, Article ID 865024, 8 pages
http://dx.doi.org/10.1155/2013/865024

Research Article

Cytotoxic Effect of Nanocrystalline $MgFe_2O_4$ Particles for Cancer Cure

S. Kanagesan,[1] M. Hashim,[1] S. Tamilselvan,[2] N. B. Alitheen,[2] I. Ismail,[1] and G. Bahmanrokh[1]

[1] *Materials Synthesis and Characterization Laboratory (MSCL), Institute of Advanced Technology (ITMA), Universiti Putra Malaysia, 43400 Serdang, Selangor, Malaysia*
[2] *Department of Cell and Molecular Biology, Faculty of Biotechnology and Biomolecular Sciences, Universiti Putra Malaysia, 43400 Serdang, Selangor, Malaysia*

Correspondence should be addressed to S. Kanagesan; kanagu1980@gmail.com

Received 30 August 2013; Accepted 16 October 2013

Academic Editor: William W. Yu

Nanocrystalline magnesium ferrites ($MgFe_2O_4$) were produced with an average grain size of about 20 nm. Their structural, morphological, and magnetic characterizations were studied. The cytotoxic effects of $MgFe_2O_4$ nanoparticles in various concentrations (25, 50, 100, 200, 400, and 800 μg/mL) against MCF-7 human breast cancer cells were analyzed. MTT assay findings suggest the increased accumulation of apoptotic bodies with the increasing concentration of $MgFe_2O_4$ nanoparticles in a dose-dependent manner. Flow cytometry analysis shows that $MgFe_2O_4$ nanoparticles in 800 μg/mL concentration are more cytotoxic compared to vehicle-treated MCF-7 cells and suggests their potential utility as a drug carrier in the treatment of cancer.

1. Introduction

Recent research interests on spinel ferrites are due to their unique optical, electrical, and magnetic properties. These characteristics are strongly dependent on their size, shape, and dispersion [1]. Study of spinel ferrite MFe_2O_4 (where M = Fe, Mn, Zn, Co, Mg, Cu, Ni) nanoparticles has great significance in modern technologies such as contrast enhancement of magnetic resonance imaging, high density data storage, and magnetic carriers for site-specific drugs delivery [2]. Amongst the spinel ferrite families, magnesium ferrite ($MgFe_2O_4$) is a soft magnetic n-type semiconducting material [3, 4].

The spinel ferrite particles synthesized by solid-state methods show an assembly of irregular shapes and agglomerations [5, 6]. A wide variety of methods are being used to synthesize spinel ferrite nanoparticles including gas condensation, rapid solidification, electrodeposition, sputtering, crystallization of amorphous phases, wet-chemical methods like coprecipitation, hydrothermal, sonochemical reactions, sol-gel method, combustion, reverse micelle technique, hydrothermal route, microemulsion, and mechanical attrition-ball milling [7–17]. The synthesis method plays a very important role on the physical, chemical, structural, and magnetic properties of a spinel ferrite. In the present investigation, $MgFe_2O_4$ nanoparticles are synthesized by the microemulsion technique due to its advantages over other methods like easy control of particle size and overall homogeneity. In most research reports, synthesis techniques aim to limit the size of the nanoparticle to below 30 nm and to have uniform-size distribution. These nanoparticles have extensive applications in drug delivery systems and especially in cancer therapies [18].

Breast cancer is one of the most common cancers among females worldwide and especially in Asia. Cancer can occur due to an uncontrolled cell proliferation or a reduction in cell death or both. The present treatments in cancer therapy including surgery, radiation, photodynamic therapy, and conventional chemotherapy have severe limitations; for example, they can affect all the cells in the body [19, 20]. In this regard, nanosized particles with their size comparable to that of biological structures are very smart materials for the manipulation, sensing, and detection of biological systems [21, 22]. Recent progress in utilizing inorganic nanoparticles

for biomedical applications has received more attention due to their pronounced applications [23–25]. The toxicity of nanoparticles towards diseased cells would create a new criterion for the development of their potential applications in the field of medicine [26]. There are evidential reports available in the literature demonstrating the antimicrobial and anticancer activities of silver, gold, ZnO, and TiO_2 nanoparticles [27–30]. Previous reports show that the considerable antibacterial activity of magnesium-based nanoparticles is attributed to the generation of reactive oxygen species [31, 32]. Even though $MgFe_2O_4$ nanoparticles serve as a potential agent and are used in several biological applications, their toxicity towards cancer cells is not heavily researched. Ge et al. reported the cytotoxicity of magnesium-based nanoparticles towards human umbilical vein endothelial cells [33]. Sun et al. examined the cytotoxicity of several metal oxide nanoparticles on human cardiac microvascular endothelial cells [34]. Lai et al. reported that magnesium oxide nanoparticle possesses less cytotoxic effects against human astrocytoma U87 cells [35]. More recently, Di et al. reported the promising application of magnesium-based nanoparticle in nanocryosurgery for tumor treatment [36]. Hence, the toxicity of $MgFe_2O_4$ nanoparticles towards cancer cells remains an area of potential interest. In the present study, $MgFe_2O_4$ nanoparticles are synthesized by microemulsion technique. The size, structure, morphology, and magnetic properties of the resultant ferrite powder are examined. The cytotoxic effect of the samples against human breast cancer cells is investigated in order to realize the goal of transforming cancer cell populations which will be useful for the cancer treatment in real time.

2. Experimental Techniques

2.1. Nanopowder Synthesis. Magnesium nitrate and ferric nitrate in the stoichiometric ratio of $MgFe_2O_4$ were dissolved in distilled water to form an aqueous solution. To obtain the main phase, cetyltrimethylammonium bromide (CTAB) was used as a surfactant and 1-Butanol as cosurfactant. They were mixed with the oil n-octane and continuously stirred to get a clear solution. The aqueous solution of nitrates was added to this clear solution. Tiny water droplets estimated to be 20 nm were observed in the oil. The size of the water droplets could be controlled by the molar ratio of water to surfactant [37]. Reduction agent sodium borohydrate was added to the mixture drop by drop under vigorous stirring to get a black precipitate. The liquid mixture was stirred for 10 minutes, centrifuged, and washed by ethanol several times to remove the surfactant and oil. The precursor was then heated at 150°C in a hot air oven for 24 hours. The structure analysis of the calcined samples was identified using an X-ray diffractometer (Phillips Expert ProPW3040) using Cu-K_α radiation in a wide range of 2θ ($10 < 2\theta < 80$). The particle morphology observation of the specimens was performed using a transmission electron microscope (TEM). The magnetic characteristics of the specimen were measured at room temperature using a vibrating sample magnetometer (VSM) (VSMmodelLDJ9600).

2.2. MTT 3-(4,5-Dimethyl Thaiazol-2-ve)-2-5-diphenyl Tetrazolium Bromide Assay. Cells were grown in 96-well microtiter plates (1×10^4 cells/well) containing Dulbecco's Modified Eagle Medium (DMEM) and incubated for 24 h in the presence of various concentrations of $MgFe_2O_4$ nanoparticles. After the incubation, the medium was removed and 25 μL of the MTT (5 mg of MTT dissolved in 1 mL of phosphate-buffered saline) and 175 μL of fresh medium were added to each well. The plates were incubated for a further 4 h at 37°C under 5% CO_2 in a humidified incubator. After incubation, the medium was removed from all the wells. The formazan crystals that formed were then solubilized in 200 μLs of dimethyl sulfoxide (DMSO). The colored solution was quantified at 575 nm using a microplate reader. The cell viability was determined as percent of the control. Each condition was performed in triplicate wells and data were obtained from at least 3 separate experiments.

2.3. Trypan Blue Exclusion Test. Cell viability was determined by the trypan blue exclusion test after cells were harvested with designated treatments in different concentration of $MgFe_2O_4$ nanoparticles using trypan blue. Equal amounts of cell suspension and 0.4% trypan blue were mixed for 1-2 min and 10 microliter of the mixture was taken to the hemocytometer and the cells were counted in all the four fields under a light microscope.

2.4. Acridine Orange/Propidium Iodine (AO/PI) Staining. Apoptosis induced by treating with various concentrations of $MgFe_2O_4$ nanoparticles was assayed using AO/PI (Sigma-Aldrich). Cells were incubated with various concentrations of $MgFe_2O_4$ nanoparticles for 24 h in 6-well tissue culture plates. The cells were washed with phosphate buffer saline (PBS) after removing the media. Fresh media were added in each well and the cells were stained for 10 min by adding 10 μL of AO/PI mix (10 mg mL^{-1} AO and 10 mg mL^{-1} PI in PBS). The cells were washed with PBS and observed under a fluorescence microscope (Nikon ECLIPSE, TS100, Tokyo) with an excitation filter of 480/30 nm.

2.5. Annexin V-PI Staining. To determine the induction of apoptosis in magnesium ferrite nanoparticle treated MCF-7 cells, FITC-labeled annexin V staining (FITC Annexin V Apoptosis Detection Kit, BD Pharmingen, NJ) was performed. The cells were treated with various concentrations of $MgFe_2O_4$ nanoparticle for 24 h and stained as per manufacturer's instructions. Simultaneously, the cells were stained with PI to differentiate the necrotic cells from the apoptotic cells. The stained cells were analyzed using FACSCalibur (BD Biosciences, NJ, USA) flow cytometer, and Cell Quest Prosoftware.

3. Result and Discussions

3.1. Thermal Study. Figure 1 shows the thermogravimetric analysis (TGA) curve of the magnesium ferrite precursor examined from room temperature to 1,200°C in air with a heating rate of 10°C per minute. The study of mass loss

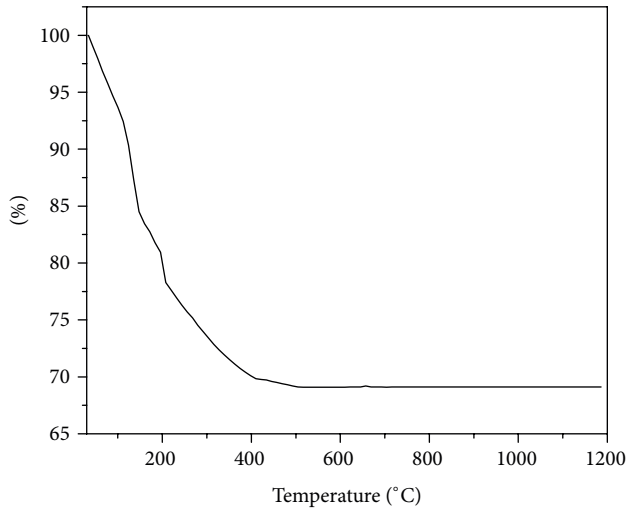

Figure 1: TGA curve of magnesium ferrite gel heated at a rate of 10°C/min in air.

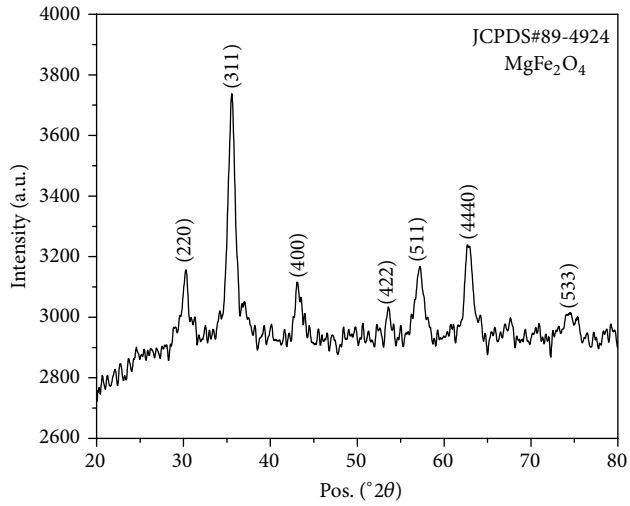

Figure 2: XRD pattern of magnesium ferrite powder calcined at 150°C for 24 hours.

of the sample with the temperature increase is useful in determining the absorbtion of water, sample purity, carbonate content, removal of organic impurity, and the decomposition reactions. The decomposition process consists of three regions. They are 50–150°C, 150–220°C, and 220–400°C. The initial weight loss from 28 to 150°C is due to the removal of physically adsorbed water [38]. The second weight loss in the temperature range of 150–220°C is due to the dehydration of OH group in NO_3^- constituent, the oxidation of complexes, and formation of semiorganic carbon metal/metal oxide [39, 40]. The third stage of weight loss occurs between 220 and 400°C. This is due to the formation of equivalent metal oxides and the spinel phase [41, 42]. There is no weight loss observed above 400°C. This indicates the formation of pure magnesium ferrite. The net weight loss is found to be 42.77% in the temperature range of 30 to 1200°C and the maximum weight loss takes place before 200°C.

3.2. Structural Studies. Figure 2 shows XRD pattern of magnesium ferrite powder heat treated at 150°C for 24 hours. The diffraction peaks agree with the international standard diffraction data card, JCPDS number 89-4924, and provide a clear evidence of $MgFe_2O_4$ formation. This indicates the existence of a cubic spinel structure. The most intense reflections observed at 2θ values of 35.56, 43.09, 53.58, 57.21, 62.69, and 74.57 are assigned to (220), (311), (400), (422), (511), (440), and (533) planes of cubic spinel structure. This lattice parameter is determined to be 8.366 Å. The line broadening of the X-ray diffraction pattern gives a clear evidence for the nanometer range of the synthesized powder.

3.3. Morphological Analysis. $MgFe_2O_4$ particles generally have spherical shape with smooth surfaces with a narrow size distribution. Figure 3 shows the typical TEM images of calcined $MgFe_2O_4$ powder. It can be seen from the TEM image that the particles are spherical in shape with uniform size distribution. The size of these particles is controllable to 20 nm in

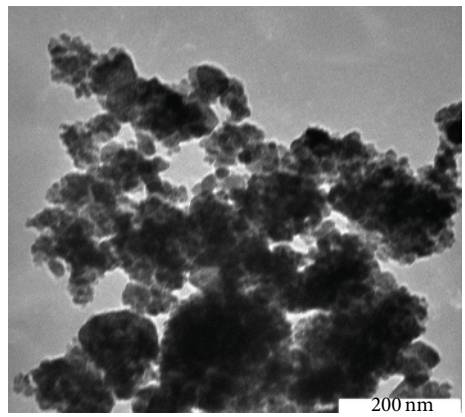

Figure 3: Particle morphology of magnesium ferrite powder heat treated at 150°C for 24 hours.

diameter. This is in good agreement with the size determined by Scherrer's formula from X-ray diffraction studies.

3.4. FTIR Spectra. The transmittance spectra of the sample calcined at 150°C for 24 h are presented in Figure 4. The band observed at 3446 cm^{-1} is due to the symmetric stretching vibrations of O–H groups and the bands at 1638 and 1121 cm^{-1} are attributed to the symmetric stretching vibrations of hydrogen-bonded surface water molecules [43], which indicate the absorbed or free water presence in the samples [44]. These vibrations confirm the fact that hydroxyl groups are still reserved in the samples and are not entirely removed even after the samples were calcined at 200°C [45]. The characteristic band at 1380 cm^{-1} is ascribed to the symmetric vibration of NO_3^- group. The sharp band at 997 cm^{-1} is more significant in Mg-based ferrite [46]. The absorption peaks corresponding to 997 and 710 cm^{-1} are related to the presence of Fe ions in ferrites [47]. Generally, the metal oxide vibrations occur below 1000/cm. The band around 475 cm^{-1}

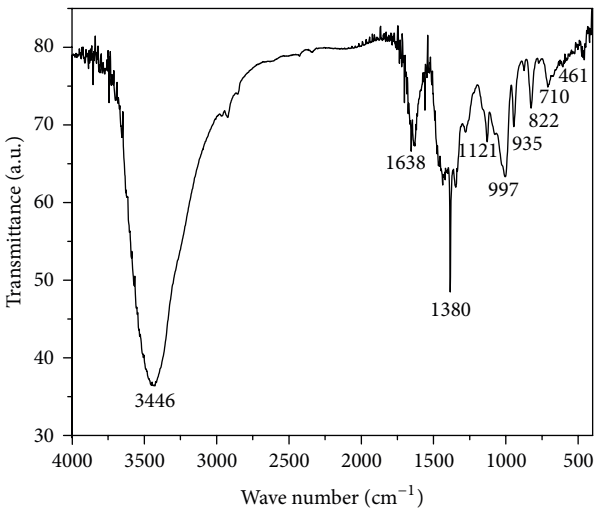

Figure 4: FT-IR spectra of magnesium ferrite powder calcined at 150°C for 24 h.

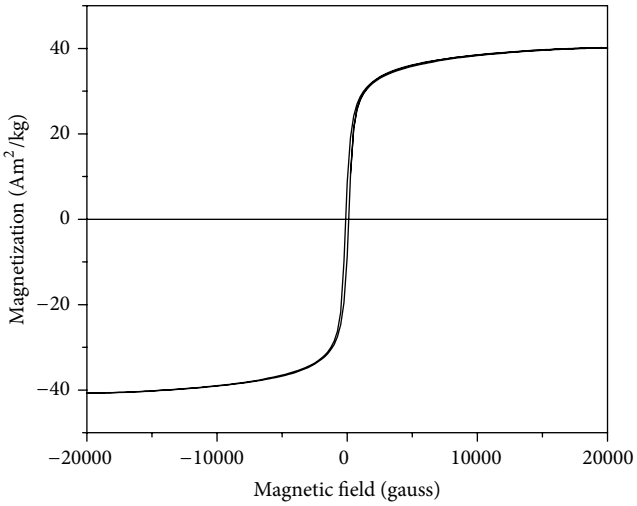

Figure 5: Hysteresis curve of sample heat treated at 150°C for 24 h.

ascribed to the intrinsic vibration of octahedral sites, typical to spinel structure characteristics, confirms that the samples prepared are spinel in structure [48–50].

3.5. Magnetic Measurements. Magnetic hysteresis curve of $MgFe_2O_4$ powder measured by the vibrating sample magnetometer at room temperature is shown in Figure 5. From this graph it is observed that the sample exhibits ferromagnetic behavior at room temperature [51]. The value of maximum saturation magnetization as found from hysteresis loop is 40 Am^2/kg. This value is lower than that reported for the bulk nickel ferrite but it is higher than the reported values for bulk $MgFe_2O_4$ and $CuFe_2O_4$ [5, 52]. This ferrite powder exhibits a coercivity value of 112 Gauss. Structural and magnetic properties of spinel ferrites are believed to be dependent on several factors including the method of preparation, chemical composition, particles size, shape, magnetization direction,

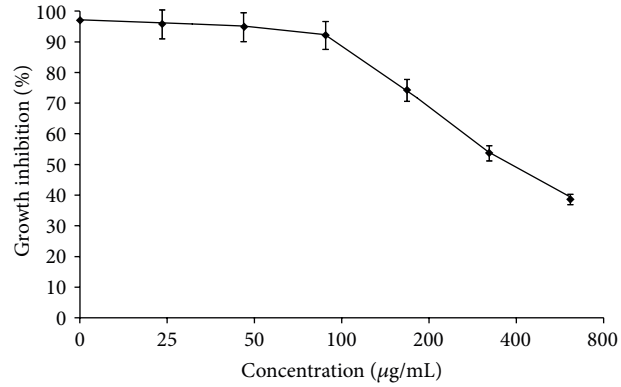

Figure 6: Effect of $MgFe_2O_4$ on growth of breast cancer cell lines MCF-7. Cells are seeded in 96-well plates and incubated with different concentrations of $MgFe_2O_4$ and noted after 24 h maintaining at 37°C. Cell viabilities are determined by 3-(4,5-dimethylthiazol-2-yl)-2,5-diphenyl tetrazolium bromide (MTT) assay. Data points are presented as means ± SD of triplicate experiments.

and crystallinity [53, 54]. In addition, the hysteresis loops showed that M_s is not saturated, which indicates the existence of surface spin disorder of nanoparticles [53].

3.6. Cytotoxicity and Induction of Apoptosis by $MgFe_2O_4$. Human breast epithelial MCF-7 cells were exposed to $MgFe_2O_4$ nanoparticles at the concentrations of 25, 50, 100, 200, 400, and 800 μg/mL for 24 h and cytotoxicity was determined using MTT assays. The cell viability in MTT assay significantly reduced to 95%, 94%, 91%, 72%, 50%, and 34% for the concentrations of 25, 50, 100, 200, 400, and 800 μg/mL, respectively ($P < 0.05$). The variation of cell viabilities with respect to $MgFe_2O_4$ concentration is shown in Figure 6. This variation is also supported by the previous experimental results in which the magnesium nanoparticle shows toxicity at only higher concentrations [33, 55].

The MCF-7 cells were preferentially selected for the toxicity analysis induced by magnesium ferrite nanoparticles to provide insights to breast cancer investigations. The MCF-7 cells treated with various concentrations of $MgFe_2O_4$ nanoparticles were examined by fluorescence microscopy after AO/PI staining. The magnetic nanoparticles induced apoptosis. The structural and morphological changes of the cells were studied. In general, morphological changes, such as cell shrinkage and condensed and fragmented chromatin, are associated with apoptotic cell death [56]. Figure 7 shows the AO/PI staining results obtained using fluorescence microscopy. As seen in Figure 7, control cells do not show any apoptotic bodies. The cells treated with increasing concentrations of $MgFe_2O_4$ nanoparticle show a progressive accumulation of the apoptotic bodies in a dose-dependent manner.

The apoptotic cell death in MCF-7 cells induced by $MgFe_2O_4$ nanoparticle was confirmed and subsequently quantified by flow cytometric analysis. Early apoptotic cells can easily be identified by green fluorescence of FITC-conjugated annexin V, as annexin V has a high affinity toward phosphatidyl serine (PS) residues which are externalized from

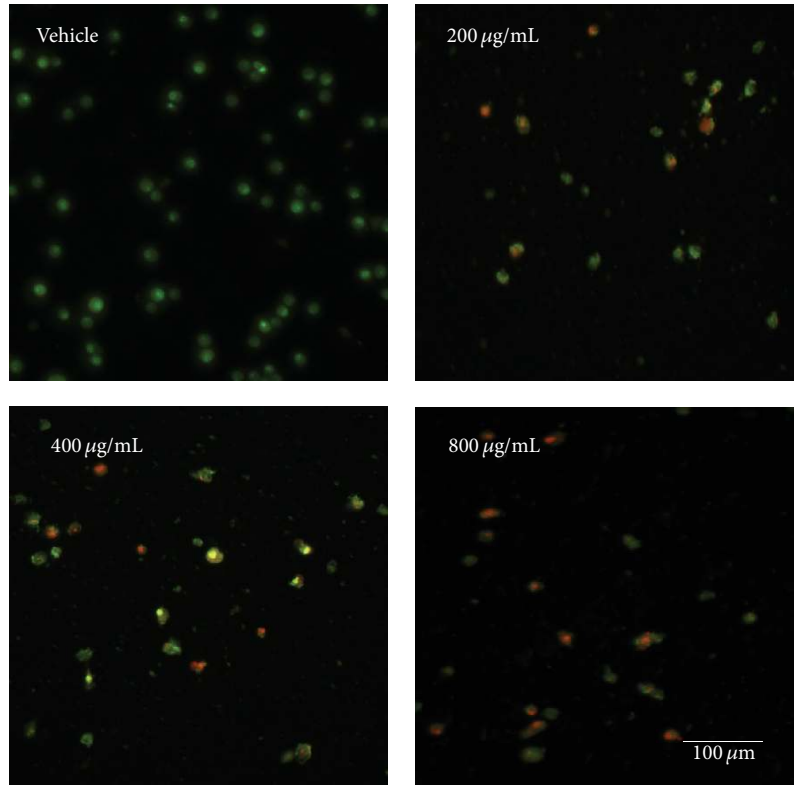

Figure 7: Morphological assessment of MCF-7 cells stained with acridine orange (green) and propidium iodine (red). Cells are incubated with or without $MgFe_2O_4$ at various concentrations for 24 h. Cells with intact membrane and stained green indicate viable cells; cells that are stained orange represent secondary necrotic or late apoptotic cells containing fragmented DNA (magnification 100x, scale bar 100 μm).

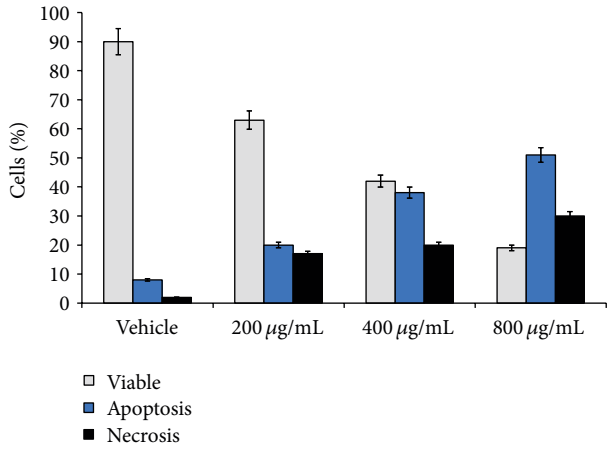

Figure 8: Flow cytometry analysis of untreated and treated MCF-7 cells with $MgFe_2O_4$ for 24 h stained with Annexin V-FITC/PI. Each bar represents the population of viable, apoptotic, and necrotic cells of three independent experiments.

inner to outer leaflet of the plasma membrane during early stages of apoptosis [57, 58]. Figure 8 shows the results of flow cytometric analysis of FITC-annexin V-PI stained MCF-7 cells treated with different concentrations of magnesium ferrite. The percentages of apoptotic and necrotic population in treated and untreated cells were calculated from the flow cytometric data and the results clearly show the dose-dependent reduction in cell viability of MCF-7 cells in the presence of $MgFe_2O_4$. Most importantly, the apoptotic and necrotic population in MCF-7 cells increased by 37%, 58%, and 81% in presence of 200, 400, and 800 μg/mL of $MgFe_2O_4$, respectively. The results of flow cytometric analysis clearly establish the efficient induction of apoptotic and necrotic cell death in MCF-7 cells by $MgFe_2O_4$ (Figure 8). While necrosis is a form of cell death resulting from direct cell damage, apoptosis is a form of cell programmed cell death where one or more cells effectively commit suicide [59]. Our study demonstrated the simultaneous visualization of viable, necrotic, and apoptotic cells in any given sample suggesting that $MgFe_2O_4$ nanoparticle induces apoptosis and necrosis in a dose-dependent manner. In the present case, the observed cytotoxic effects are more difficult to diagnose but are possibly due to free radical generation through Fenton and/or Haber-Weiss reactions whose effects only become noticeable at higher intracellular concentrations of iron [60]. The morphological changes in the cells may be due to cytotoxicological and phenotypic effects of magnesium oxide internalization. This may have drastically impeded transcriptional regulation and protein synthesis resulting in loss of cell phenotype and possibly cell death. In order to evaluate these possibilities, further studies into the physiochemical basis of the observed $MgFe_2O_4$ cytotoxicity are necessary.

4. Conclusions

$MgFe_2O_4$ nanoparticles were successfully synthesized by the microemulsion technique. XRD analysis reveals that the synthesized samples have a single cubic spinel phase without trace of any impurity. The size of the $MgFe_2O_4$ powder, as observed from TEM image, is controllable to 20 nm in diameter. The FTIR pattern confirms the characteristic peaks of ferrite system. The hysteresis loop exhibits ferromagnetic behavior. The toxicity of $MgFe_2O_4$ nanoparticles towards MCF-7 human breast cancer cells was demonstrated. The cell death was observed by apoptosis and necrosis and the cytotoxicity results show dose-dependent toxicity of $MgFe_2O_4$ nanoparticles toward cancer cells. These findings reveal the potential utility of $MgFe_2O_4$ nanoparticles in cancer therapy due to their toxicity towards MCF-7 cells.

Conflict of Interests

The authors declare that they have no conflict of interests.

References

[1] J. Hu, T. W. Odom, and C. M. Lieber, "Chemistry and physics in one dimension: synthesis and properties of nanowires and nanotubes," *Accounts of Chemical Research*, vol. 32, no. 5, pp. 435–445, 1999.

[2] Z. L. Wang, Y. Liu, and Z. Zhang, *Handbook of Nanophase and Nanostructured Materials*, vol. 3, Kluwer Academic/Plenum, New York, NY, USA, 2003.

[3] R. J. Willey, P. Noirclerc, and G. Busca, "Preparation and characterization of magnesium chromite and magnesium ferrite aerogels," *Chemical Engineering Communications*, vol. 123, pp. 1–16, 1993.

[4] N. Sivakumar, A. Narayanasamy, J.-M. Greneche, R. Murugaraj, and Y. S. Lee, "Electrical and magnetic behaviour of nanostructured $MgFe_2O_4$ spinel ferrite," *Journal of Alloys and Compounds*, vol. 504, no. 2, pp. 395–402, 2010.

[5] H. Deng, H. Chen, and H. Li, "Synthesis of crystal MFe_2O_4 (M = Mg, Cu, Ni) microspheres," *Materials Chemistry and Physics*, vol. 101, no. 2-3, pp. 509–513, 2007.

[6] S.-H. Yu and M. Yoshimura, "Direct fabrication of ferrite MFe_2O_4 (M = Zn, Mg)/Fe composite thin films by soft solution processing," *Chemistry of Materials*, vol. 12, no. 12, pp. 3805–3810, 2000.

[7] J. Rockenberger, E. C. Scher, and A. P. Alivisatos, "A new nonhydrolytic single-precursor approach to surfactant-capped nanocrystals of transition metal oxides," *Journal of the American Chemical Society*, vol. 121, no. 49, pp. 11595–11596, 1999.

[8] T. Hyeon, "Chemical synthesis of magnetic nanoparticles," *Chemical Communications*, vol. 9, no. 8, pp. 927–934, 2003.

[9] N. R. Jana, Y. Chen, and X. Peng, "Size- and shape-controlled magnetic (Cr, Mn, Fe, Co, Ni) oxide nanocrystals via a simple and general approach," *Chemistry of Materials*, vol. 16, no. 20, pp. 3931–3935, 2004.

[10] S. Komarneni, E. Fregeau, E. Breval, and R. Roy, "Hydrothermal preparation of ultrafine ferrites and their sintering," *Journal of the American Ceramic Society*, vol. 71, p. C-26, 1998.

[11] Q. Chen, A. J. Rondinone, B. C. Chakoumakos, and Z. John Zhang, "Synthesis of superparamagnetic $MgFe_2O_4$ nanoparticles by coprecipitation," *Journal of Magnetism and Magnetic Materials*, vol. 194, no. 1, pp. 1–7, 1999.

[12] K. Suresh, N. R. S. Kumar, and K. C. Patil, "A novel combustion synthesis of spinel ferrites, orthoferrites and garnets," *Advanced Materials*, vol. 3, no. 3, pp. 148–150, 1991.

[13] A. S. Albuquerque, J. D. Ardisson, and W. A. A. Macedo, "A study of nanocrystalline NiZn-ferrite-SiO_2 synthesized by sol-gel," *Journal of Magnetism and Magnetic Materials*, vol. 192, no. 2, pp. 277–280, 1999.

[14] N. S. Gajbhiye, S. Prasad, and G. Balaji, "Experimental study of hopkinson effect in single domain $CoFe_2U_4$ particles," *IEEE Transactions on Magnetics*, vol. 35, no. 4, pp. 2155–2161, 1999.

[15] H. F. Yu and A. M. Gadalla, "Preparation of $NiFe_2O_4$ powder by spray pyrolysis of nitrate aerosols in NH_3," *Journal of Materials Research*, vol. 11, no. 3, pp. 663–670, 1996.

[16] N. Moumen and M. P. Pileni, "Control of the size of cobalt ferrite magnetic fluid," *Journal of Physical Chemistry*, vol. 100, no. 5, pp. 1867–1873, 1996.

[17] C. Liu, B. Zou, A. J. Rondinone, and Z. J. Zhang, "Chemical control of superparamagnetic properties of magnesium and cobalt spinel ferrite nanoparticles through atomic level magnetic couplings," *Journal of the American Chemical Society*, vol. 122, no. 26, pp. 6263–6267, 2000.

[18] Q. A. Pankhurst, J. Connolly, S. K. Jones, and J. Dobson, "Applications of magnetic nanoparticles in biomedicine," *Journal of Physics D*, vol. 36, no. 13, pp. R167–R181, 2003.

[19] J. Huang, H. Li, W. Chen et al., "Dielectric barrier discharge plasma in Ar/O_2 promoting apoptosis behavior in A549 cancer cells," *Applied Physics Letters*, vol. 99, no. 25, Article ID 253701, 2011.

[20] K. Karthikeyan, A. Babu, S.-J. Kim, R. Murugesan, and K. Jeyasubramanian, "Enhanced photodynamic efficacy and efficient delivery of Rose Bengal using nanostructured poly(amidoamine) dendrimers: potential application in photodynamic therapy of cancer," *Cancer Nanotechnology*, vol. 2, no. 1–6, pp. 95–103, 2011.

[21] J. L. Arias, L. H. Reddy, and P. Couvreur, "Fe_3O_4/chitosan nanocomposite for magnetic drug targeting to cancer," *Journal of Materials Chemistry*, vol. 22, no. 15, pp. 7622–7632, 2012.

[22] N. K. Singh, S. K. Singh, D. Dash, B. P. Purkayastha, J. K. Roy, and P. Maiti, "Nanostructure controlled anti-cancer drug delivery using poly(ε-caprolactone) based nanohybrids," *Journal of Materials Chemistry*, vol. 22, pp. 17853–1763, 2012.

[23] M. Premanathan, K. Karthikeyan, K. Jeyasubramanian, and G. Manivannan, "Selective toxicity of ZnO nanoparticles toward Gram-positive bacteria and cancer cells by apoptosis through lipid peroxidation," *Nanomedicine*, vol. 7, no. 2, pp. 184–192, 2011.

[24] P. Sanpui, A. Chattopadhyay, and S. S. Ghosh, "Induction of apoptosis in cancer cells at low silver nanoparticle concentrations using chitosan nanocarrier," *ACS Applied Materials and Interfaces*, vol. 3, no. 2, pp. 218–228, 2011.

[25] C. R. Patra, R. Bhattacharya, and P. Mukherjee, "Fabrication and functional characterization of goldnanoconjugates for potential application in ovarian cancer," *Journal of Materials Chemistry*, vol. 20, no. 3, pp. 547–554, 2010.

[26] K. M. Reddy, K. Feris, J. Bell, D. G. Wingett, C. Hanley, and A. Punnoose, "Selective toxicity of zinc oxide nanoparticles to prokaryotic and eukaryotic systems," *Applied Physics Letters*, vol. 90, no. 21, Article ID 213902, 2007.

[27] A. Niu, Y. Han, J. Wu, N. Yu, and Q. Xu, "Synthesis of one-dimensional carbon nanomaterials wrapped by silver nanoparticles and their antibacterial behavior," *The Journal of Physical Chemistry C*, vol. 114, pp. 12728–1235, 2010.

[28] W. Zhou, X. Liu, and J. Ji, "Fast and selective cancer cell uptake of therapeutic gold nanorods by surface modifications with phosphorylcholine and Tat," *Journal of Materials Chemistry*, vol. 22, pp. 13969–13976, 2012.

[29] M. Ahamed, M. J. Akhtar, M. Raja et al., "ZnO nanorod-induced apoptosis in human alveolar adenocarcinoma cells via p53, survivin and bax/bcl-2 pathways: role of oxidative stress," *Nanomedicine*, vol. 7, no. 6, pp. 904–913, 2011.

[30] P. Thevenot, J. Cho, D. Wavhal, R. B. Timmons, and L. Tang, "Surface chemistry influences cancer killing effect of TiO_2 nanoparticles," *Nanomedicine*, vol. 4, no. 3, pp. 226–236, 2008.

[31] S. Makhluf, R. Dror, Y. Nitzan, Y. Abramovich, R. Jelinek, and A. Gedanken, "Microwave-assisted synthesis of nanocrystalline MgO and its use as a bacteriocide," *Advanced Functional Materials*, vol. 15, no. 10, pp. 1708–1715, 2005.

[32] K. Krishnamoorthy, G. Manivannan, S. J. Kim, K. Jeyasubramanian, and M. Premanathan J, "Antibacterial activity of MgO nanoparticles based on lipid peroxidation by oxygen vacancy," *Journal of Nanoparticle Research*, vol. 14, no. 1063, 2012.

[33] S. Ge, G. Wang, Y. Shen et al., "Cytotoxic effects of MgO nanoparticles on human umbilical vein endothelial cells in vitro," *IET Nanobiotechnology*, vol. 5, no. 2, pp. 36–40, 2011.

[34] J. Sun, S. Wang, D. Zhao, F. H. Hun, L. Weng, and H. Liu, "Cytotoxicity, permeability, and inflammation of metal oxide nanoparticles in human cardiac microvascular endothelial cells," *Cell Biology and Toxicology*, vol. 27, no. 5, pp. 333–42, 2011.

[35] J. C. K. Lai, M. B. Lai, S. Jandhyam et al., "Exposure to titanium dioxide and other metallic oxide nanoparticles induces cytotoxicity on human neural cells and fibroblasts," *International Journal of Nanomedicine*, vol. 3, no. 4, pp. 533–545, 2008.

[36] D. R. Di, Z. Z. He, Z. Q. Sun, and J. Liu, "A new nano-cryosurgical modality for tumor treatment using biodegradable MgO nanoparticles," *Nanomedicine*, vol. 8, no. 8, pp. 1233–141.

[37] G. Bahmanrokha, M. Hashima, N. Soltani et al., "High coercivity sized controlled cobalt-gold core-shell nano-crystals prepared by reverse microemulsion," *Materials Research Bulletin*, vol. 48, no. 10, pp. 4039–4047, 2013.

[38] S. Kanagesan, S. Jesurani, R. Velmurugan, M. Sivakumar, C. Thirupathi, and T. Kalaivani, "Synthesis and magnetic properties of conventional and microwave calcined barium hexaferrite powder," *Journal of Materials Science*, vol. 23, no. 2, pp. 635–639, 2012.

[39] C.-Y. Zhang, X.-Q. Shen, J.-X. Zhou, M.-X. Jing, and K. Cao, "Preparation of spinel ferrite $NiFe_2O_4$ fibres by organic gel-thermal decomposition process," *Journal of Sol-Gel Science and Technology*, vol. 42, no. 1, pp. 95–100, 2007.

[40] P. Sivakumar, R. Ramesh, A. Ramanand, S. Ponnusamy, and C. Muthamizhchelvan, "Synthesis, studies and growth mechanism of ferromagnetic $NiFe_2O_4$ nanosheet," *Applied Surface Science*, vol. 258, no. 17, pp. 6648–6652, 2012.

[41] S. Zahi, "Nickel-zinc ferrite fabricated by sol-gel route and application in high-temperature superconducting magnetic energy storage for voltage sag solving," *Materials and Design*, vol. 31, no. 4, pp. 1848–1853, 2010.

[42] P. Sivakumar, R. Ramesh, A. Ramanand, S. Ponnusamy, and C. Muthamizhchelvan, "Synthesis and study of magnetic properties of $NiFe_2O_4$ nanoparticles by PVA assisted auto-combustion method," *Journal of Materials Science*, vol. 23, pp. 1011–1015, 2012.

[43] J. Chandradass, A. H. Jadhav, K. H. Kim, and H. Kim, "Influence of processing methodology on the structural and magnetic behavior of $MgFe_2O_4$ nanopowders," *Journal of Alloys and Compounds*, vol. 517, pp. 164–169, 2012.

[44] S. Thankachan, S. Xavier, B. Jacob, and E. M. Mohammed, "A comparative study of structural, electrical and magnetic properties of magnesium ferrite nanoparticles synthesised by sol-gel and co-precipitation techniques," *Journal of Experimental Nanoscience:*, vol. 8, no. 3, pp. 347–357, 2013.

[45] A. N. Pathan, K. Sangshetti, and A. A. G. Pangal, "Synthesis, Characterisation and magnetic studies of $Co_{0.6}Zn_{0.4-x}CuxFe_2O_4$ Nanoparticles," *International of Journal Nanotechnology & Nanosciences*, vol. 1, pp. 8–12, 2010.

[46] M. Y. Salunkhe, D. S. Choudhary, and D. K. Kulkarni, "Infrared absorption studies of the system $Sr_2Me_2Fe_{12}O_{22}$," *Vibrational Spectroscopy*, vol. 34, no. 2, pp. 221–224, 2004.

[47] V. A. Potakova, N. D. Zverv, and V. P. Romanov, "On the cation distribution in $Ni_1—x—yFe_x^{2+}Zn_yFe_2^{3+}$ spinel ferrites," *Physica Status Solidi A*, vol. 12, no. 2, pp. 623–627, 1972.

[48] J. Chandradass, A. H. Jadhav, K. H. Kim, and H. Kim, "Influence of processing methodology on the structural and magnetic behavior of $MgFe_2O_4$ nanopowders," *Journal of Alloys and Compounds*, vol. 517, pp. 164–169, 2012.

[49] Y. Ahn, E. J. Choi, and E. H. Kim, "Superparamagnetic relaxation in cobalt ferrite nanoparticles synthesized from hydroxide carbonate precursors," *Reviews on Advanced Materials Science*, vol. 5, p. 477, 2003.

[50] N. Wu, L. Fu, M. Su, M. Aslam, K. C. Wong, and V. P. Dravid, "Interaction of fatty acid monolayers with cobalt nanoparticles," *Nano Letters*, vol. 4, no. 2, pp. 383–386, 2004.

[51] H. Stablein and E. P. Wohlfarth, Eds., *Ferromagnetic Materials*, 3 North-Holland, 1982.

[52] J. Smit and H. P. J. Wijn, *Ferrites Physical Properties of Ferromagnetic Oxides in Relation To Their Technical Applications*, Wiley, New York, NY, USA, 1959.

[53] P. Sivakumar, R. Ramesh, A. Ramanand, S. Ponnusamy, and C. Muthamizhchelvan, "Preparation of sheet like polycrystalline $NiFe_2O_4$ nanostructure with PVA matrices and their properties," *Materials Letters*, vol. 65, no. 9, pp. 1438–1440, 2011.

[54] A. Pradeep, P. Priyadharsini, and G. Chandrasekaran, "Sol- gel route of synthesis of nanoparticles of $MgFe_2O_4$ and XRD, FTIR and VSM study," *Journal of Magnetism and Magnetic Materials*, vol. 320, no. 21, pp. 2774–2779, 2008.

[55] G.-F. Yang, X.-H. Li, Z. Zhao, and W.-B. Wang, "Preparation, characterization, in vivo and in vitro studies of arsenic trioxide Mg-Fe ferrite magnetic nanoparticles," *Acta Pharmacologica Sinica*, vol. 30, no. 12, pp. 1688–1693, 2009.

[56] T. T. Mai, J. Moon, Y. Song et al., "Ginsenoside F2 induces apoptosis accompanied by protective autophagy in breast cancer stem cells," *Cancer Letters*, vol. 321, no. 2, pp. 144–153, 2012.

[57] S. J. Martin, C. P. M. Reutelingsperger, A. J. McGahon et al., "Early redistribution of plasma membrane phosphatidylserine is a general feature of apoptosis regardless of the initiating stimulus: inhibition by overexpression of Bcl-2 and Abl," *Journal of Experimental Medicine*, vol. 182, no. 5, pp. 1545–1556, 1995.

[58] G. Koopman, C. P. M. Reutelingsperger, G. A. M. Kuijten, R. M. J. Keehnen, S. T. Pals, and M. H. J. Van Oers, "Annexin V for flow cytometric detection of phosphatidylserine expression on B cells undergoing apoptosis," *Blood*, vol. 84, no. 5, pp. 1415–1420, 1994.

[59] N. Ueda and S. V. Shah, "Apoptosis," *Journal of Laboratory and Clinical Medicine*, vol. 124, no. 2, pp. 169–177, 1994.

[60] M. Symons and J. Gutteridge, *Free Radicals and Iron: Chemistry, Biology and Medicine*, Oxford University Press, London, UK, 1998.